2023 IEEE International Conference on Electrical Systems for Aircraft, Railway, Ship Propulsion and Road Vehicles & International Transportation Electrification Conference (ESARS-ITEC) | 979-8-3503-4689-3/23/$31.00 ©2023 IEEE | DOI: 10.1109/ESARS-ITEC57127.2023.10114846

Minimization of DC-Link Capacitance in Voltage Source Rectifiers through Nonlinear Controls Based on Lyapunov's Direct Method

Mark Vygoder, Robert M. Cuzner, Brian S. R. Armstrong
Dept. Of Electrical Engineering
University of Wisconsin Milwaukee
Milwaukee, WI, USA
mvygoder@uwm.edu, robcuzer@ieee.org, BSRA@uwm.edu

***Abstract*—The increased switching frequency offered by Silicon Carbide (SiC) based Multi-chip Power Modules may allow designers to reduce the size and weight of passive elements while still meeting converter specifications. For the 3-phase Voltage Source Rectifier (VSR), as switching frequency increases, the DC-link capacitor may be reduce while maintaining the same voltage ripple. However, an often overlooked part in sizing the DC-link capacitance is the converter's stability. The use of conventional control methods, such PI-based controls, may lead to larger DC-link capacitance to prevent instability, minimizing the value proposition of Wide Band Gap-based power conversion. Applications like electrified shipboard or more electrical aircraft can be extremely sensitive to increases in size/weight due to limited space and/or significant annualized fuel costs. To this end, this paper explores, through simulation, a nonlinear control method based on Lyapunov's direct method published 25 years ago to minimize DC-link capacitance of an SiC-based VSR.**

***Index Terms*—Voltage Source Rectifier, Nonlinear controls, Lyapunov Theory, AC/DC PWM rectifier.**

I. Introduction

The value proposition of Wide bandgap (WBG)-based power converters may not be able to be fully realized without the implementation of nonlinear controls, particularly for power converters which have nonlinear dynamics such as the 3 phase AC-to-DC Voltage Source Rectifier (VSR). The VSR is a common topology implemented in synchronous rectification, due to the availability to configure multiple multi-chip power modules (MCMP) in half-bridges to form a 3-phase VSR.

Applications such a more electric aircraft (MEA) and electrified shipboard can be extremely sensitive to size and weight. Every kilogram that can be saved off of a power converter can result in millions of USD in annualized fuel savings and every liter of size savings can improve usable space in naval vessels.

As Silicon-Carbide (SiC)-based MCMP begin to replace IGBT-based MCMP, higher switching frequencies are available for designs at higher current levels. These higher switching frequencies may allow designers to reduce the size power quality filters, and by doing so, improve power density (kW/L) and gravimetric density (kW/kg) (though EMC filters must also be considered in the overall design with increased edge rates and switching frequencies).

This work was partially sponsored by the NAVFAC Naval Shore Energy Technology Transition and Integration (NSETTI) program

The sizing of the DC-link capacitance for a VSR (shown in Fig. 1) breaks down into a few criteria: DC voltage ripple, capacitor rms current ripple, and controller stability/transient performance during load steps/rejection or feeding downstream constant power loads. DC voltage ripple is approximately given:

$$C = \frac{P_{Load}}{v_{dc}\Delta v_{dc} f_{sw}} \tag{1}$$

Examples of analytical solutions for capacitor rms current ripple can be found in [1]–[3], though not address in this paper.

An often overlooked part is the value of DC capacitance needed to ensure stability of the VSR. Shi *et. al.* [4] derives requirements for DC-link capacitances based on linearization of the dq model around an operating point (Lyapunov's indirect method). This method used conventional cascaded PI controls and where the VSR was feeding a resistive load. VSRs feeding constant power loads may need different DC capacitor sizing, or more specific control bandwidth requirement, but this serves as a good starting point. The inequality from [4] to size DC capacitance for stability is given by:

$$C \geq \frac{20}{m_{d-low}^2 R_{min}} L \tag{2}$$

where m_{d-low} is the minimum d-axis modulation index needed to account for variations in input voltage, L is the boost inductance, and R_{min} is the minimum resistance found at full load. This implies that any time the capacitance from (2) $\geq$ (1), the controls are driving the size of the DC capacitance.

To illustrate this point further with a quantitative example, Fig. 2a shows the trade-space of capacitor values that satisfy (1) for switching frequency ranging from 50 to 100 kHz and for the power rating ranging from 100 to 250 kW. The system has a 800 V bus and assumes a 2% voltage ripple.

Equation (2) is dependent on the boost inductance of the VSR. To size L, voltage harmonics were generated for asymmetrically-sampled PWM from [5]. Then, the inductance

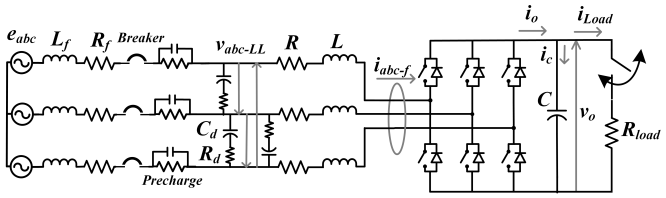

Fig. 1. Voltage Source Rectifier Diagram

TABLE I
CRITERIA FOR ESTABLISHING DIFFERENT TYPES OF STABILITY.

Type of Stability	**Mathematical Properties of V and $\dot{V}$**			
	V is PD	$\dot{V}$ is NSD	$\dot{V}$ is ND	V is radially unbounded
Lyapunov	✓	✓		
Asymptotic	✓		✓	
Global Lyapunov	✓	✓		✓
Global Asymptotic	✓		✓	✓

values were iteratively increased to meet a current harmonic distortion (IHD) requirement of 5% with an input voltage of 480 Vac. The values for L acrpss the trade-space are shown in Fig. 2b.

Next, these values for L were next plugged into (2) resulting in Fig. 2c, which appears to be roughly independent of the target power rating, and mostly dependent on switching frequency. This is due to both L and R_{min} decreasing simultaneously as power increases. Still, clearly, the values of capacitance in Fig. 2a is less than Fig. 2c across the trade-space.

To this end, this paper applies a nonlinear controlled based on Lyapunov's direct method from [6] to help minimized the increased DC capacitance and there by helping to maximize the value proposing of WBG-based power conversion equipment.

A. Non-linearity of VSR

The large-signal average state-space equation for a VSR (ignoring the feeder cable and capacitive filter with damping) is given by [4], [6], [7]:

$$e_{abc}(t) = L\frac{d}{dt}i_{abc}(t) + Ri_{abc}(t) + \frac{1}{2}m_{abc}(t)v_o(t) \quad (3)$$

$$\frac{1}{2}i_{abc}(t)^T m_{abc}(t) = i_{load}(t) + C\frac{d}{dt}v_o(t) \quad (4)$$

A nonlinear term can be seen on the right hand side of (3). Term $\frac{1}{2}m_{abc}(t)v_o(t)$ is nonlinear as input control variables are multiplied with a system state variable. In particular, this is the DC voltage that the VSR is trying to maintain. While in linear time-invariant (LTI) systems, of canonical form $\dot{\mathbf{x}}(t) = A\mathbf{x}(t) + B\mathbf{u}(t)$, the state vector, $\mathbf{x}(t)$ and input vector, $\mathbf{u}(t)$ are added together.

In a Voltage Source Inverter (VSI), $v_o(t)$ is typically represented by an ideal voltage source, making term constant, no longer changing with time, and thus, linear. In an example of a VSR is charging batteries, the battery voltage still changes with time, but the stiffness of the battery voltage mean the system dynamics are slower and thus easier to control than compared to a DC-link capacitor of a VSR feeding a DC distribution system or a back-end of a motor drive. Lastly, the term $\frac{1}{2}i_{abc}(t)^T m_{abc}(t)$, in (4) is nonlinear as well.

Further, the VSR is a boost rectifier. The AC-to-DC VSR and DC-to-DC boost converter are both non-minimum phase systems. Such systems mean that the inverse plant model is unstable. In an LTI systems, a non-minimum phase systems contain right-hand plane zero, which is the case if the equation of the VSR or DC-DC boost converter are linearized. If one were to design a controller based on an inverse plant model, said controller would be unstable , where further design techniques may need to be implemented. This right hand plane zero dynamic comes from the dynamics of the boost converter, where an increase in bus voltage requires an increase the duty cycle, which requires the bottom switch to stay on longer to build energy in the inductor. During this time, energy is not being transferred to the DC bus and the DC voltage continuous to fall. This type of behavior is typical of right-hand plane zero system. In summary, the VSR is a *nonlinear non-minimum phase*, time-invariant system.

Various methods for controls of nonlinear time-invariant systems are laid out by Slotine and Li in [8] and have been applied to the VSR such as: 1.) Lyapunov's direct method [6]; 2.) Lyapunov's indirect method (linearization around an operation point) [4]; 3.) Feedback linearization [9]; 4.) Sliding-Mode Control (SMC) [10].

B. Lyapunov Theory

Lyapunov's direct method can be used to establish different levels of stability based different criteria one is able to prove. These criteria are shown in Table I, where V is known as the Lyapunov function, $\dot{V}$ is the total derivative of V, and are functions of state-space variables $\mathbf{x}$. For example, to establish Lyapunov stability, one must show that $V(\mathbf{x})$ is positive definite (PD) $\forall \mathbf{x} \neq \mathbf{0}$, and that $\dot{V}(\mathbf{x})$ is negative semi-definite (NSD) $\forall \mathbf{x}$. The inability to show that a candidate Lyapunov function does not meet certain criteria does not mean the physical system is unstable, only that a different Lyapunov function may be required to establish stability.

To establish asymptotic stability, $\dot{V}(\mathbf{x})$ must be shown to be negative definite (ND) $\forall \mathbf{x} \neq \mathbf{0}$. Asymptotic stability ensures that the $\mathbf{x} \to \mathbf{0}$ as time approaches infinity. However, asymptotic stability but does not give how *much* time it will take for $\mathbf{x} \to \mathbf{0}$, only that it does eventually. It is important to note that Lyapunov stability does not establish that $\mathbf{x} \to \mathbf{0}$, only that the system's states are bounded by some limit, and therefore, the system's energy will not approach infinity, i.e, instability.

Lastly to establish global Lyapunov stability or global asymptotic stability (as opposed to local Lyapunov or asymptotic stability), radial unboundedness must be shown by $V(\mathbf{x}) \to \infty$ as $|\mathbf{x}| \to \infty$. This condition removes certain types of functions like $V(x) = 1/(x+1)$.

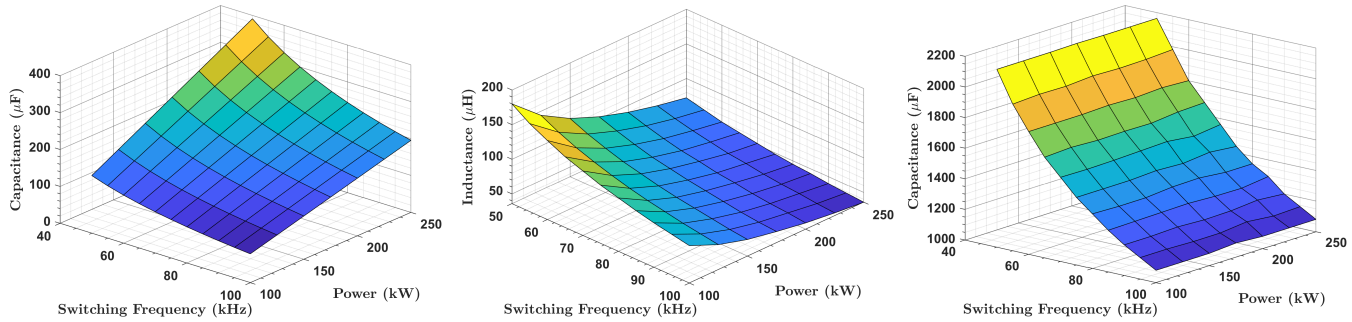

(a) (b) (c)

Fig. 2. (a) Capacitance values required to meet 2% voltage ripple, (b) Inductance values required to 5% IHD. (c) Capacitance values requires to meet (2).

TABLE II
REVIEW OF LYAPUNOV-BASED CONTROLLERS

Ref.	Year	Topology and Filter
[6]	1998	3-phase VSR
[11]	2006	3-phase NPC VSR
[12]	2006	1-phase VSI, active power filter
[13]	2008	3-phase CSI
[14]	2014	1-phase VSI with LCL filter, grid-forming UPS
[15]	2015	1-phase VSI with LCL filter, grid-following
[16]	2018	3-phase/4-wire, 4-pole NPC, Active power filter
[17]	2019	3-phase, VSI with LCL filter, grid-following
[18]	2019	3-phase, 2-pole NPC with LCL filter, grid-following
[19]	2020	1-phase, 7-level Casacaded H-bridge VSR

C. Review of Lyapunov-based Controls

H. Komurcugil and O. Kukrer published a lyapunov-based controller in 1998 for a VSR with a boost inductor. The controller contains 3 main parts: 1.) feedforward, 2.) i_d^* reference generation, and 3.) feedback.

The feedforward is based on the steady-state dq model of a VSR to derive the steady-state modulation signals from the reference command. The reference generation calculates id^* based on off DC-side load current. The error correction uses a control law that was derived from establishing global asymptotic stability through Lyapunov's direct model.

After the publishing of [6], Komurcugil *et. al.* and others have applied similar control methods to different topologies (1-phase VSI/VSR, 3-phase VSI, current source inverters (CSI), and Neutral Point Clamped (NPC) converters) across different applications (UPS/grid-forming, grid-following, and active power filtering) and with different power quality filter structures (L, LC, and LCL). A summary of this literature is tabulated in Table II.

II. DERIVATION OF VSR CONTROLLER

This section reproduces the derivation presented in [6]. The state-space model of a VSR in dq frame is given as:

$$L\frac{d}{dt}i_d = e_d - Ri_d - \frac{1}{2}v_o m_d + \omega L i_q \tag{5a}$$

$$L\frac{d}{dt}i_q = e_q - Ri_q - \frac{1}{2}v_o m_q - \omega L i_d \tag{5b}$$

$$C\frac{d}{dt}v_o = \frac{3}{4}(m_d i_d + m_q i_q) - i_{load} \tag{5c}$$

The modulation signals in dq frame (m_{dq}) are defined as:

$$m_{dq} = M_{dq} + \Delta m_{dq} \tag{6}$$

where M_{dq} are the feed-forward signals and Δm_{dq} are the error correction terms.

A. Feed-forward Terms

Starting with the feed-forward terms, if we assume the system is in steady-state, the left hand side (LHS) of (5) will equal 0. Additionally, the system signals will equal the reference values. So,

$$\begin{aligned} v_d &= v_d^*, \quad i_d = i_d^*, \quad i_q = i_q^*, \\ v_o &= v_o^*, \quad m_d = M_d, \quad m_q = M_q \end{aligned} \tag{7}$$

Plugging the signals in steady-state as defined in (7) in (5) with LHS=0 gives:

$$0 = e_d - Ri_d^* - \frac{1}{2}v_o^* M_d + \omega L i_q^* \tag{8a}$$

$$0 = e_q - Ri_q^* - \frac{1}{2}v_o^* M_q - \omega L i_d^* \tag{8b}$$

$$0 = \frac{3}{4}(M_d i_d^* + M_q i_q^*) - i_{load} \tag{8c}$$

Assuming the VSR is running at unity power factor ($i_q^* = 0$), and is synchronized to the input voltage ($e_q = 0$) solving for M_d and M_q gives:

$$M_d = \frac{2(v_d^* - Ri_d^*)}{v_o^*} \tag{9}$$

$$M_q = -\frac{2\omega L i_d^*}{v_o^*} \tag{10}$$

These constants can either be pre-computed around rated conditions, or updated with the control loop, with the trade-off of sensor noise injection into the control loop.

B. i_d^* Generation

Plugging (9) into (8c) gives:

$$i_{load} = \frac{3}{2v_o^*}\left(v_d^* i_d^* - R i_d^{*^2}\right) \tag{11}$$

Assuming unity power factor operation does simplify this equation.

Solving for i_d^* from (11) gives:

$$i_d^* = \frac{1}{2}\left[\frac{v_d^*}{R} \pm \sqrt{\left(\frac{v_d^*}{R}\right)^2 - \frac{8 v_o^* i_{load}}{3R}}\right] \tag{12}$$

Equation (12) gives two solutions but one will typically be larger than the max current rating and therefore discarded.

C. Error-correction terms

The error correction terms are solved for by choosing control laws where the Lyapunov derivative satisfies the negative definite condition required to establish asymptotic stability. The Lyapunov function is chosen as:

$$V(\mathbf{x}(t)) = \frac{3}{2}Lx_1(t)^2 + \frac{3}{2}Lx_2(t)^2 + Cx_3(t)^2 \tag{13}$$

where

$$\mathbf{x}(t) = \begin{bmatrix} x_1(t) & x_2(t) & x_3(t) \end{bmatrix}^T \tag{14}$$

and

$$x_1(t) = i_d(t) - i_d(t)^* \tag{15a}$$
$$x_2(t) = i_q(t) - i_q(t)^* \tag{15b}$$
$$x_3(t) = v_o(t) - v_o(t)^* \tag{15c}$$

The explicit time dependence of the error signals are shown as the Lyapunov derivative is a total derivative with respect to time, and will be:

$$\dot{V}(\mathbf{x}) = 3x_1 L\dot{x_1} + 3x_2 L\dot{x_2} + 2x_3 C\dot{x_3} \tag{16}$$

The explicit time dependence notation will be dropped for simplicity. The derivatives of $\mathbf{x}$:

$$\dot{x_1} = \dot{i_d} \tag{17a}$$
$$\dot{x_2} = \dot{i_q} \tag{17b}$$
$$\dot{x_3} = \dot{v_o} \tag{17c}$$

as the derivatives of the reference signals equal zero since i_{dq}^* and v_o^* are DC values. Rearranging (15):

$$i_d = x_1 + i_d^* \tag{18a}$$
$$i_q = x_2 + i_q^* \tag{18b}$$
$$v_o = x_3 - v_o^* \tag{18c}$$

Plugging in (17a), (18a),(18c), (9), and (6) into (5a) gives:

$$L\dot{x_1} = \omega L x_2 - R x_1 - \frac{1}{2}v_o^* \Delta m_d - \frac{(V_d^* - R I_d^*)}{V_o^*}x_3 - \frac{1}{2}x_3 \Delta m_d \tag{19}$$

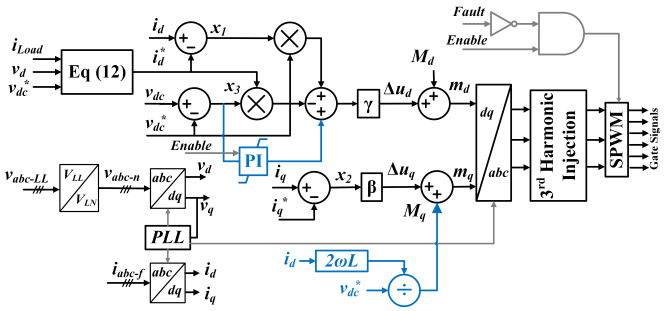

Fig. 3. Modified Lyapunov-based controller based on [6].

Plugging in (17b), (18b),(18c), (10), and (6) into (5b) gives:

$$L\dot{x_2} = -\omega L x_1 - R x_2 - \frac{1}{2}v_o^* \Delta m_q - \frac{\omega L I_d^*}{V_o^*}x_3 - \frac{1}{2}x_3 \Delta m_q \tag{20}$$

Plugging in (17c), (18a), (18b), (9), (10), and (6) into (5c) gives:

$$C\dot{x_3} = \frac{3}{4}\left[\frac{2(v_d^* - R i_d^*)}{v_o^*}x_1 + i_d^* \Delta m_q + \Delta m_d x_1 - \frac{2\omega L i_d^*}{v_o^*}x_2 + \Delta m_q x_2\right] \tag{21}$$

Plugging in the equations for $L\dot{x_1}$, $L\dot{x_2}$, $C\dot{x_3}$ back into (16), terms cancel and simplify to:

$$\dot{V}(\mathbf{x}) = -\frac{3}{2}\left(v_o^* x_1 - i_d^* x_3\right)\Delta m_d - \frac{3}{2}v_o^* x_2 \Delta m_q - 3R(x_1^2 + x_2^2) \tag{22}$$

The selection for Δm_{dq} is made such that $\dot{V}(\mathbf{x})$ is N.D., and is given by:

$$\begin{aligned} \Delta m_d &= \gamma(v_o^* x_1 - i_d^* x_3), & \gamma > 0 \\ \Delta m_q &= \beta x_2, & \beta > 0 \end{aligned} \tag{23}$$

γ and β can be thought of as proportional gains, and also serve as scaling factors if the signals are not converted into per unit, as in this case. To double check the N.D. of $\dot{V}(\mathbf{x})$, (23) is plugged back into (22), which gives

$$\dot{V}(\mathbf{x}) = -\frac{3}{2}\gamma\left(v_o^* x_1 - i_d^* x_3\right)^2 - \frac{3}{2}\beta v_o^* x_2^2 - 3R(x_1^2 + x_2^2) \tag{24}$$

Verifying 3 conditions are met for global asymptotic stability:

1) $V(\mathbf{x})$ from (13) is P.D. $\forall \mathbf{x} \neq \mathbf{0}$.
2) $\dot{V}(\mathbf{x})$ is N.D. $\forall \mathbf{x} \neq \mathbf{0}$ as shown by (24).
3) $V(\mathbf{x})$ is radially unbounded, and shown by $V(\mathbf{x}) \to \infty$ as $|\mathbf{x}| \to \infty$

It should be noted that Lyapunov's direct method may not address cross-coupling behavior, and one may need to add decoupling terms into the control law based on the plants dynamics. Fig. 3 shows the final controller. The blue lines highlight differences between the controller in [6]. Mainly, integral action was added to drive voltage error to zero. The q-axis feed-forward term, M_q, was modified by used measured i_d instead of a predetermined operating point to help reduce dq cross-coupling. Even though integral action was added,

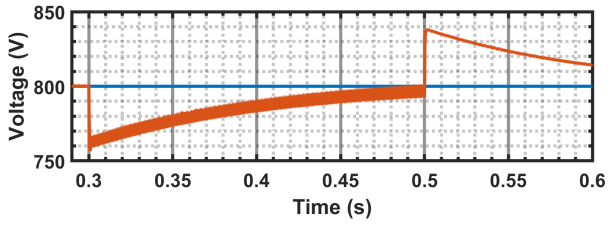

Fig. 4. Conventional PI Controller, $C = 2200\mu F$, load step and load rejection.

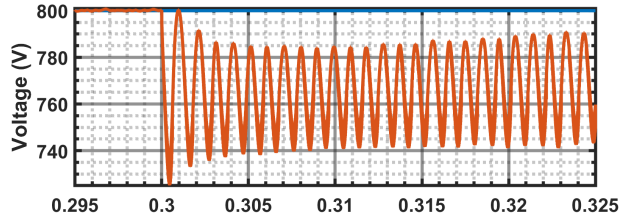

(a)

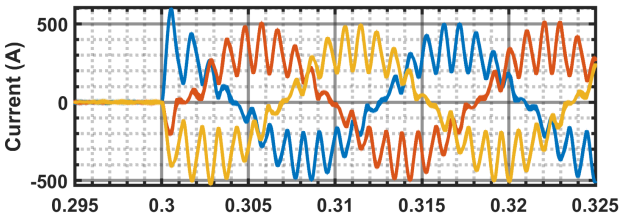

(b)

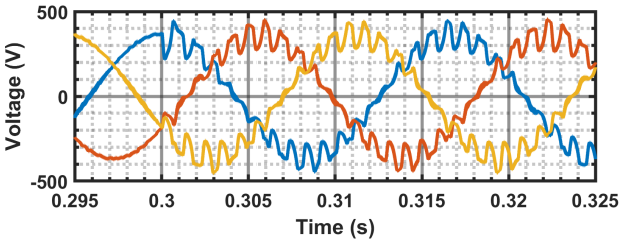

(c)

Fig. 5. Convention PI Controller with $C = 1100\mu F$ during load step: (a) v_{dc}, (b) i_{abc}, (c) v_{abc}.

the control effort from the integrator is significantly reduced compared to conventional cascaded PI controls.

III. Simulation Results

Time-domain simulations were executed in Matlab/Simulink 2019b (solver: Runga-Kutta ode4, time-step: 200 ns). The switch frequency and power rating used were 50 kHz and 200 kW, respectively. The controller update rate was 10 μs, implementing asymmetric sampling. Simulation parameters can be found in Table III.

It should be noted that often times, the source voltage (e_{abc}) is placed right at the output of the converter filter without any impedance between the source and converter. This leads to a perfectly stiff source, which may not be representative of realistic conditions, and may lead to unrealistically good sim-

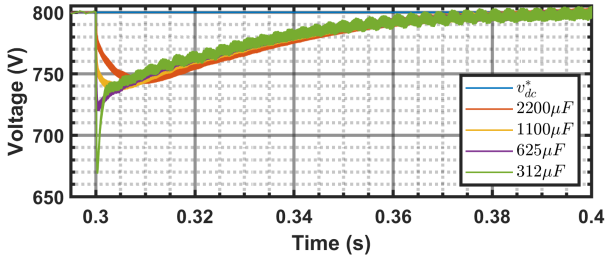

(a)

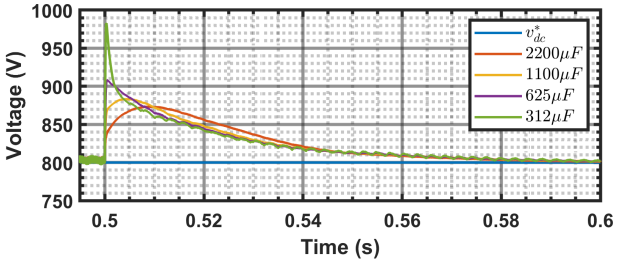

(b)

Fig. 6. v_{dc} response of Lyapunov Controller as C is reduced: (a) load step, (b) load rejection.

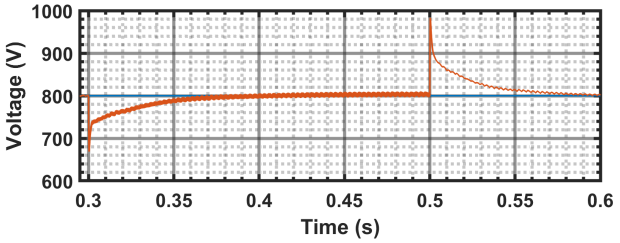

(a)

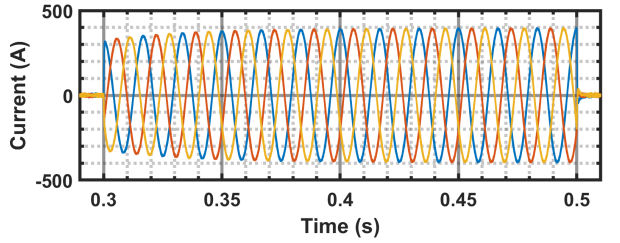

(b)

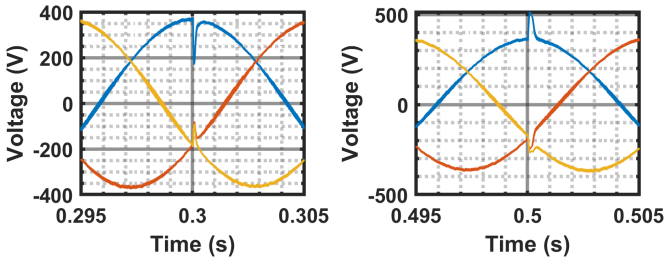

(c) (d)

Fig. 7. Lyapunov Controller as $C = 312\mu F$: (a) v_{dc}, (b) i_{abc}, (c) v_{abc} during load step (d) v_{abc} during load rejection.

TABLE III
SIMULATION PARAMETERS AND SIGNALS

Symbol	Description	Value
e_{abc}	input 3-phase voltage	480 $V_{LL}RMS$
R_f	input feeder cable resistance	1.2 mΩ
L_f	input feeder cable inductance	76 μH
C_d	filter capacitance	7.6 μF
R_d	damping resistance	3.4 Ω
R	boost inductor equivalent series resistance	50 mΩ
L	boost inductance	90 μH
C	DC-link capacitance	312-2200 μF
R_{load}	load resistance	3.2 Ω
$m_{abc}(t)$	modulation indices of each leg	-1.15 to 1.15
$i_{abc}(t)$	boost inductor currents	A
$v_o(t)$	DC-link capacitor voltage	V
$i_o(t)$	output DC current of the converter	A
$i_{load}(t)$	load current	A

ulation results. Also, some capacitance with damping is added before the boost inductor, forming an LC filter instead of just an L filter. Without the capacitor, measuring voltage between the feeder cable and boost inductor gives poor measurement quality.

Fig. 4 shows the transient response of a conventional cascaded PI controller with $C = 2200\mu F$. A 100% load step is applied at 0.3 s and the full load is removed at 0.5 s. Fig. 4 shows the controller is stable with the selected value of DC capacitance (following (2)).

Next, Fig. 5 demonstrates unacceptable performance from the conventional PI controls as the DC capacitance is halved and is now below (2). Smaller values of capacitance will cause further degraded performance and instability.

Transient responses from Lyapunov-based controller are shown in Fig. 6 for capacitance values of 312μF, 625μF, 1100μF, and 2200μF.312μF was selected, as it satisfies the 2% voltage ripple requirement. The Lyapunov-based controls are able to operate at smaller values of capacitance than the conventional cascaded PI controller. Clearly, the nonlinear is stable to recover from the load transients with 312μF of capacitance; however, the voltage dip and overshoot may be too significant to be deemed acceptable. When C is 625 μF, the undershoot/overshoot are 8% and 12.5%, respectively. Depending on the application, capacitance reduction of 2-4x is viable. Interestingly, the change in v_{dc} during load step/rejection of the conventional PI controls when C is 2200 μF is less than the nonlinear controller.

Fig. 7 shows the transient responses with $C = 312\mu F$. Fig. 7c and Fig. 7d show a zoomed view of v_{abc} during load steps and load rejection, where the voltage input experiences transients in response to the change in current draw. These transients would not have occurred if the input voltage source was placed directly at the input of the filter, and would have resulted in better, but unrealistic, transient performance. An attempt was made to take v_d measured into account for the feed-forward M_d term, but undesirable oscillations occurred.

IV. CONCLUSION

This paper shows that a nonlinear controller based off of Lyapunov's directs method from [6] enables a VSR to operate at a reduced DC capacitance that a conventional cascaded PI controller cannot, while achieving good transient performance. This mean that by updating the control scheme, potential mass and/or volume saving are possible, which can have significant implications for MEA or electrified shipboard applications. This paper also seeks to encourage other researchers and professionals in the field to not only assess controls of power conversion equipment by their transient performance, but also by their potential impact on power density and specific power.

REFERENCES

[1] J. W. Kolar and S. D. Round, "Analytical calculation of the rms current stress on the dc-link capacitor of voltage-pwm converter systems," *IEE Proceedings-Electric Power Applications*, vol. 153, no. 4, pp. 535–543, 2006.

[2] U. Ayhan and A. M. Hava, "Analysis and characterization of dc bus ripple current of two-level inverters using the equivalent centered harmonic approach," in *2011 IEEE energy conversion congress and exposition*. IEEE, 2011, pp. 3830–3837.

[3] G. Gohil, L. Bede, R. Teodorescu, T. Kerekes, and F. Blaabjerg, "Analytical method to calculate the dc link current stress in voltage source converters," in *2014 IEEE International Conference on Power Electronics, Drives and Energy Systems (PEDES)*. IEEE, 2014, pp. 1–6.

[4] B. Shi, G. Venkataramanan, and N. Sharma, "Design considerations for reactive elements and control parameters for three phase boost rectifiers," in *IEEE International Conference on Electric Machines and Drives, 2005.* IEEE, 2005, pp. 1757–1764.

[5] D. G. Holmes and T. A. Lipo, *Pulse width modulation for power converters: principles and practice*. John Wiley & Sons, 2003, vol. 18.

[6] H. Komurcugil and O. Kukrer, "Lyapunov-based control for three-phase PWM AC/DC voltage-source converters," *IEEE Transactions on Power Electronics*, vol. 13, no. 5, pp. 801–813, 1998.

[7] V. Blasko and V. Kaura, "A new mathematical model and control of a three-phase ac-dc voltage source converter," *IEEE transactions on Power Electronics*, vol. 12, no. 1, pp. 116–123, 1997.

[8] J.-J. E. Slotine, W. Li *et al.*, *Applied nonlinear control*. Prentice hall Englewood Cliffs, NJ, 1991, vol. 199, no. 1.

[9] D.-C. Lee, G.-M. Lee, and K.-D. Lee, "DC-bus voltage control of three-phase AC/DC PWM converters using feedback linearization," *IEEE transactions on industry applications*, vol. 36, no. 3, pp. 826–833, 2000.

[10] J. F. Silva, "Sliding-mode control of boost-type unity-power-factor pwm rectifiers," *IEEE transactions on industrial electronics*, vol. 46, no. 3, pp. 594–603, 1999.

[11] M. YongQing, L. Zheng, S. Wen, L. Yi, S. YanMin, and Y. Ting, "Study on Mathematical Model and Lyapunov-Based Control for Three-Level NPC Voltage-Source Rectifier," in *2006 IEEE International Symposium on Industrial Electronics*. Montreal, Que.: IEEE, Jul. 2006, pp. 1949–1954. [Online]. Available: http://ieeexplore.ieee.org/document/4078213/

[12] H. Komurcugil and O. Kukrer, "A new control strategy for single-phase shunt active power filters using a lyapunov function," *IEEE Transactions on Industrial Electronics*, vol. 53, no. 1, pp. 305–312, 2006.

[13] ——, "Control strategy for three-phase current-source inverters based on lyapunov's direct method," in *2008 IEEE International Symposium on Industrial Electronics*, 2008, pp. 890–895.

[14] H. Komurcugil, N. Altin, S. Ozdemir, and I. Sefa, "An extended lyapunov-function-based control strategy for single-phase ups inverters," *IEEE Transactions on Power electronics*, vol. 30, no. 7, pp. 3976–3983, 2014.

[15] ——, "Lyapunov-function and proportional-resonant-based control strategy for single-phase grid-connected VSI with LCL filter," *IEEE Transactions on Industrial Electronics*, vol. 63, no. 5, pp. 2838–2849, 2015.

[16] S. S. Seyedalipour, S. Bayhan, and H. Komurcugil, "Lyapunov-function-based control approach for three-level four-leg shunt active power filters with nonlinear and unbalanced loads," in *2018 IEEE 27th International Symposium on Industrial Electronics (ISIE)*. IEEE, 2018, pp. 427–432.

[17] I. Sefa, S. Ozdemir, H. Komurcugil, and N. Altin, "An enhanced Lyapunov-function based control scheme for three-phase grid-tied VSI with LCL filter," *IEEE Transactions on Sustainable Energy*, vol. 10, no. 2, pp. 504–513, 2018.

[18] N. Altin, I. Sefa, H. Komurcugil, and S. Ozdemir, "A modified lyapunov-function based control scheme for three-phase three-level two-leg grid-tied NPC inverter," in *2019 7th International Istanbul Smart Grids and Cities Congress and Fair (ICSG)*. IEEE, 2019, pp. 218–222.

[19] G. Jean-Pierre, N. Altin, A. El Shafei, and A. Nasiri, "A control scheme based on lyapunov function for cascaded h-bridge multilevel active rectifiers," in *2020 IEEE Applied Power Electronics Conference and Exposition (APEC)*. IEEE, 2020, pp. 2021–2026.